Thermo-hydromechanical behavior of Callovo-Oxfordian claystone in the framework of geological disposal of nuclear waste

Jian-Fu Shao[1]
with contributions of many members of the GEOM team and Andra

[1]University of Lille, CNRS, Centrale Lille, LaMcube, UMR9013, France

Example of French Cigeo project

Cigéo – French project of geological radioactive waste disposal

- In France, French Radioactive Waste Management Agency (Andra) is responsible for the long term management of radioactive waste produced in France
- Cigéo project is dedicated for the disposal of High Level (HLW) and Intermediate Level – Long Life (ILW-LL) wastes, if it is licensed.
  - Main level of Cigéo consists of two zones ILW-LL ($\phi \sim 10$ m) and HLW ($\phi \sim 0{,}8$ m)
  - Host rock is Callovo-Oxfordian claystone layer with ~150m thickness, ~500m depth, ~10^{-20}-10^{-21} m^2 permeability

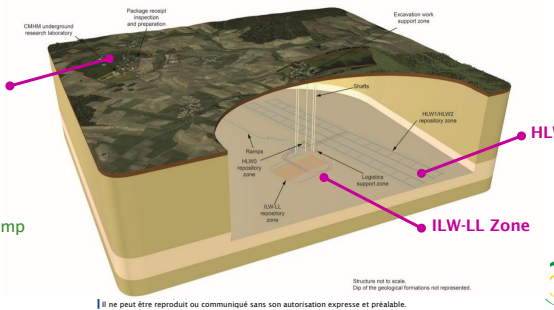

Key number
~80 km tunnel, shaft, ramp ($\phi \sim 10$ m)
~140 km micro-tunnel ($\phi \sim 1$ m)

Example of French Cigeo project-2

The Callovo-Oxfordian clay host rock formation

The Paris Basin

- General geological framework well documented (oil & water exploration)
- Classic basin structure
- Known structural context
- Stable stress orientations since 20 Ma

Callovo-Oxfordian

- Age : 160 million years
- Around 500m depth
- Thickness ≥ 120 m over a large area (230 km²)
- Very low hydraulic conductivity (<< 10^{-12} m/s)
- No tectonic fracture over a large area (230 km²)
- Small molecular diffusion
- high retention capacity for radionuclides

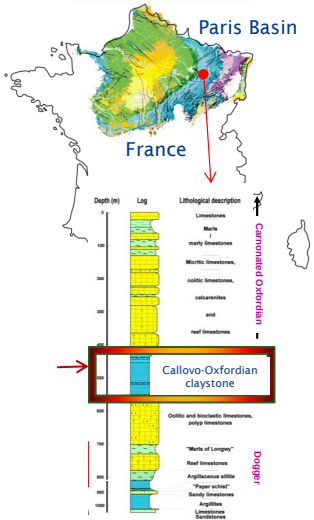

Context and motivation

- Clayey rocks investigated as host rock for geological disposal of radioactive waste in several countries,...
- Multiscale microstructure
- Plastic deformation and damage
- Strong sensitivity to water saturation change
- Time-dependent behavior
- Structural anisotropy
- Swelling and self-sealing

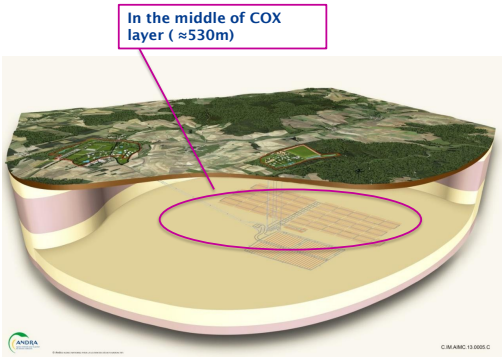

(From Armand G., Andra)

French Cigeo project - URL

Meuse/Haute Marne Underground Research Laboratory

Andra started in 2000 to build the URL for research on the feasibility of a possible deep repository

- Characterize the confining properties of the claystone Cox
- Demonstrate the constructability of the repository

Key data

- **~2 km of drifts; ~8000 m of core drillings; ~11 500 sensors, ~40 experiments**

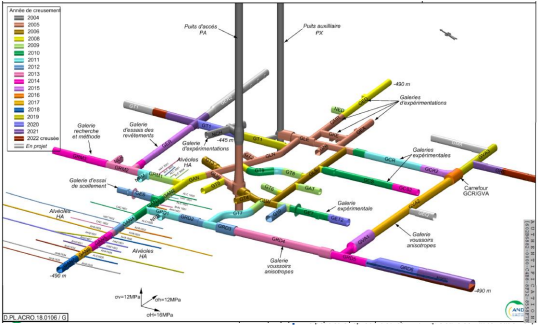

esse et préalable.

Behavior of drifts within the MHM-URL

In-situ observations – Excavation induced fractured zone/gallery closure

- Anisotropic induced fractured zone: extension is proportional to the drift diameter
- Fractured zone plays an important role for hydromechanical responses
  - Anisotropic convergence
  - Anisotropic pore pressure field around drift

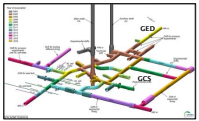

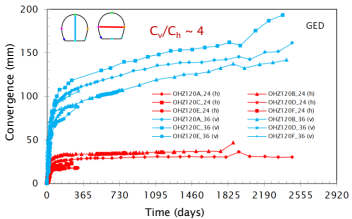

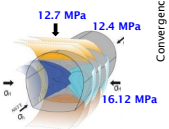

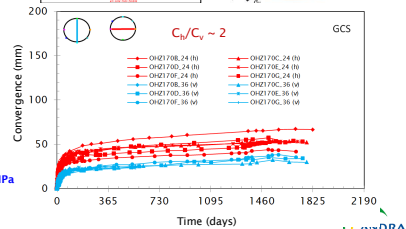

French Cigeo project - URL heating experiment

Thermal experiments in URL

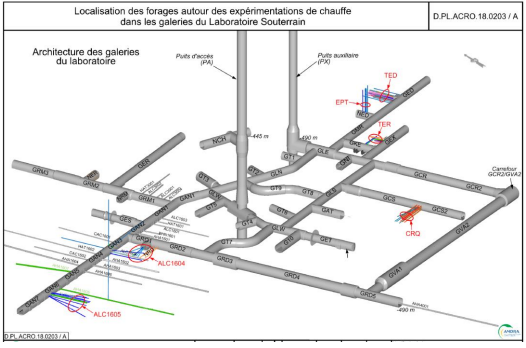

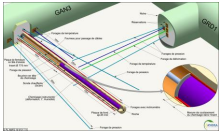

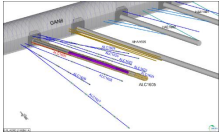

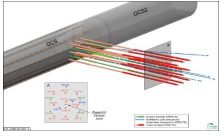

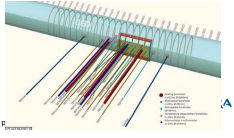

DRD/MFS/18-0176

In-situ gas injection tests into COx
Overview water/gas injection sequence

10 years of water/gas pressure monitoring :

- Gas tests were done with nitrogen
- Water permeability tests (HYDROx) have been repeated in the middle interval of PGZ1201 borehole

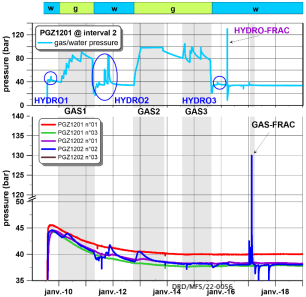

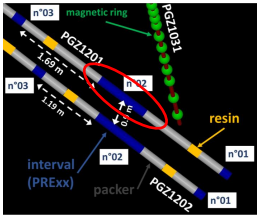

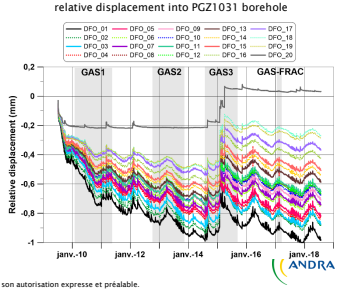

French Cigeo project

Stress/strain measurement of liner in URL

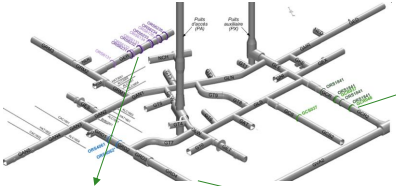

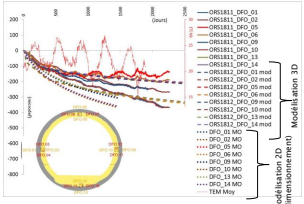

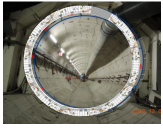

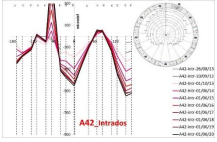

Flat jack test for stress measurement

Mineralogical compositions and microstructure

Example of Callovo-Oxfordian claystone (COx)

Callovo-Oxfordian claystone: Robinet et al., *2012*

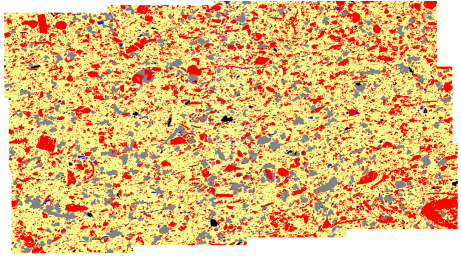

Scanning Electron Microscopy
(spatial resolution = 0,3 µm /pixel)

Carbonates
Clay matrix
Tectosilicates
Heavy minerals

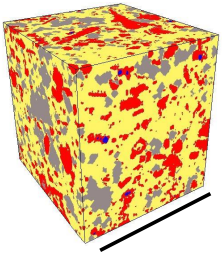

Synchrotron X-ray tomography
(spatial resolution = 0,7 µm)
180 µm

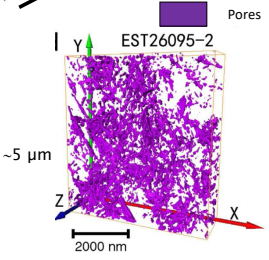

Pore network 3D – FIB SEM (*Song et al., 2015*)

Spatial variability of mineralogy - COx

Mineralogical compositions

- ✓ Clay minerals (Illite, mica, I/S, kaolinite, chlorite (20-60%)
- ✓ Tectosilicates: quartz (10-40%) and feldspars (<2%)
- ✓Carbonates: calcite (10-75%), dolomite (2-8%)…
- ✓ others: pyrite (<1%) …

Petrophysical-parameters

- ✓Density of grains : 2.69 (2.65-2.73)
- ✓ Organic materials: COT < 1,5 %
- ✓Size of pores: 10-30 nm

- The spacial variability is mainly in the vertical direction due to sedimentaion phases

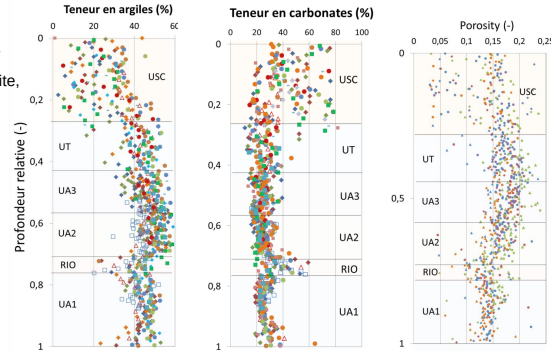

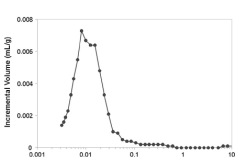

(Robinet et al. 2012)

Representative volume element for multiscale modeling

COx claystone

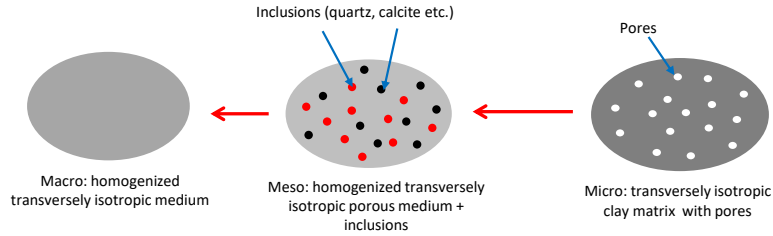

Other clayey rocks -Vaca-Muerta shale

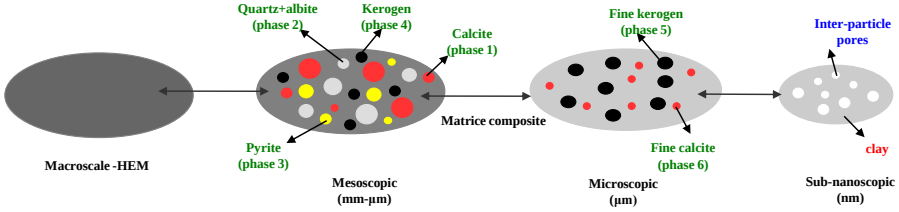

- Multi-steps homogenization techniques

Some basic mechanical properties - COx

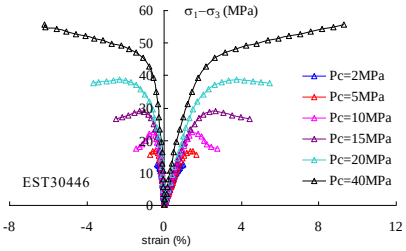

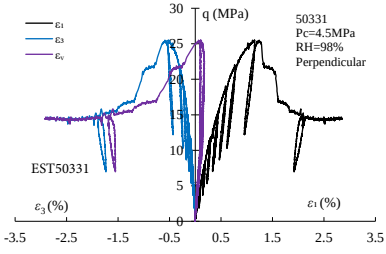

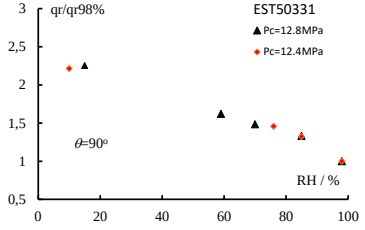

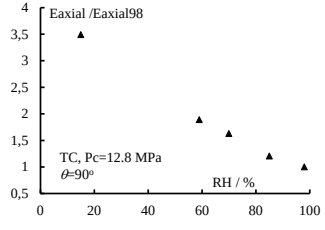

Time-dependent deformation - COx

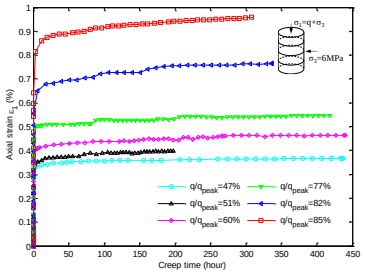

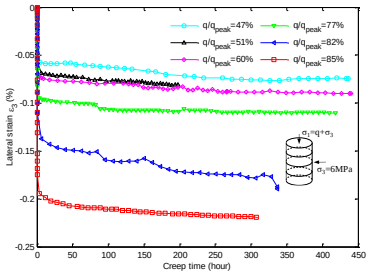

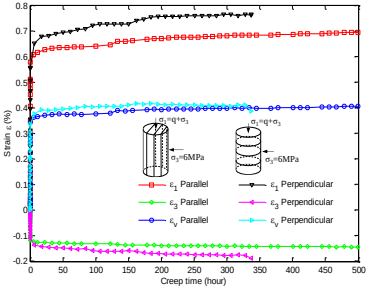

- Axial and lateral strains at different levels of deviatoric stress (Liu et al. 2015)
- Influence of structural anisotropy (Liu et al. 2015)

Micro-tomographic analysis of creep strain - COx

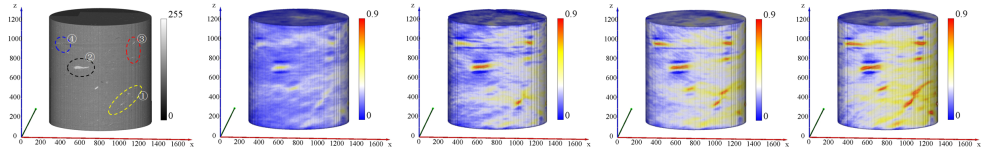

(a) Initial sample (b) $\Delta\sigma_1$=25.5 → 32.7MPa, t=6d (c) $\Delta\sigma_1$=25.5 → 32.7MPa, t=17d (d) $\Delta\sigma_1$=25.5 → 32.7MPa, t=45d (e) $\Delta\sigma_1$=25.5 → 32.7MPa, t=59d

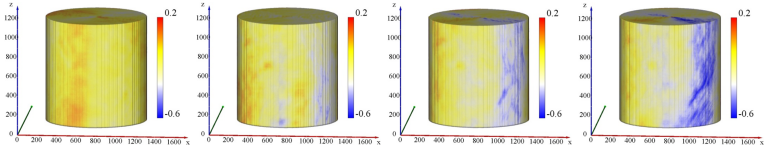

(f) $\Delta\sigma_1$=25.5 → 32.7MPa, t=6d (g) $\Delta\sigma_1$=25.5 → 32.7MPa, t=17d (h) $\Delta\sigma_1$=25.5 → 32.7MPa, t=45d (i) $\Delta\sigma_1$=25.5 → 32.7MPa, t=59d

Incremental axial and radial strain (in %) at different time during a creep test, perpendicular sample (Shi et al. 2021a, Shi et al. 2021b)

Poromechanical behavior - COx

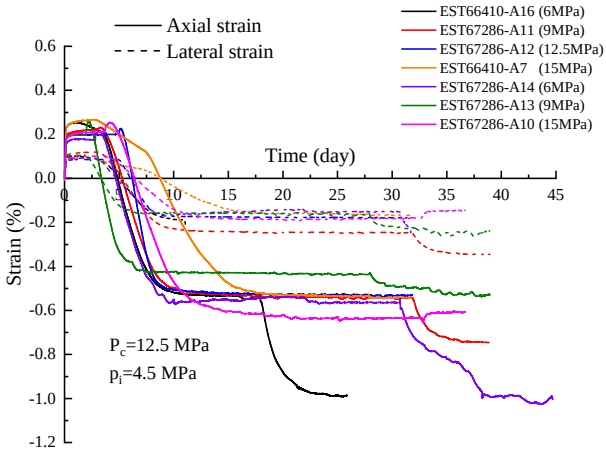

Variations of axial and lateral strain during application of confining pressure (first step); water injection (second step); readjustment of confining pressure from 12.5 MPa to a desired value (Zhang et al. 2024)

Poromechanical behavior - COx

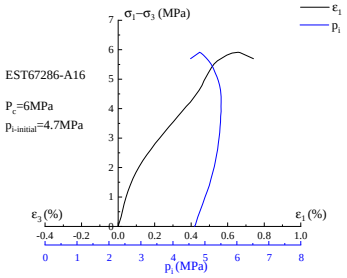

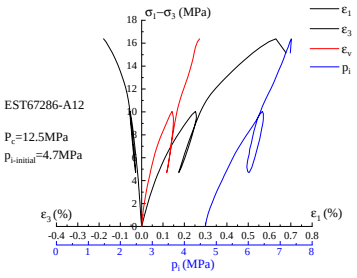

Zhao et al. 2024

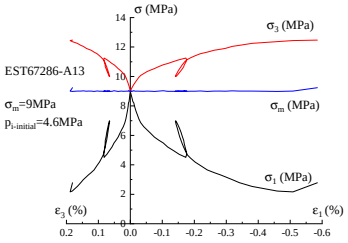

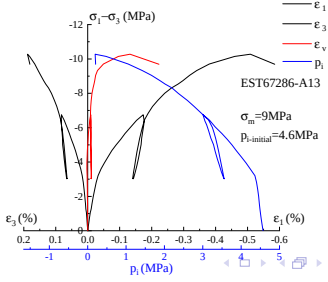

Thermal effects - COx

- Weak effect on elastic properties
- Certain effect on failure strength to be considered; mainly due to the decrease of internal friction of solid clay matrix

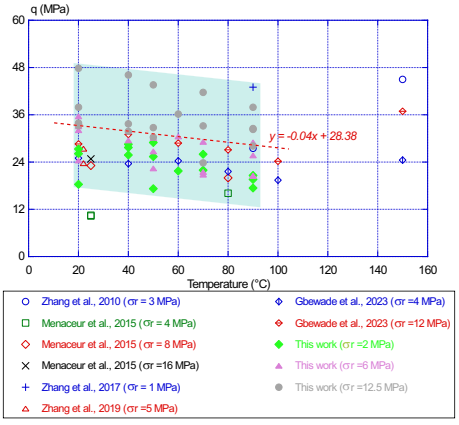

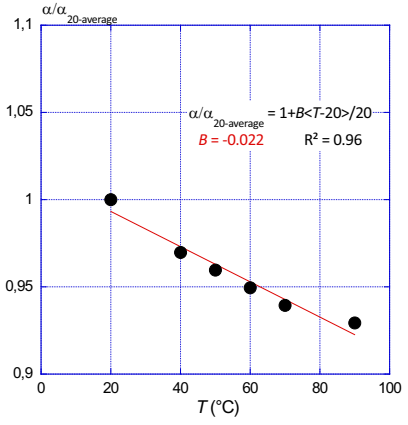

Homogenization of elastic properties of COx claystone

Consideration of anisotropic clay matrix

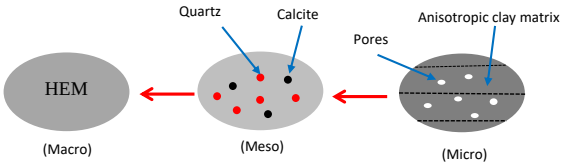

$$\boldsymbol{\sigma}^{pm} = \mathbb{C}^{pm} : \boldsymbol{\epsilon}^{e-pm} \quad , \quad \mathbb{C}^{pm} = \mathbb{C}^{s} : (\mathbb{I} - f\mathbb{A}^{p})$$

$$\mathbb{A}^{p} = (\mathbb{I} - \mathbb{P}^{p} : \mathbb{C}^{s})^{-1} : \left[(1-f)\mathbb{I} + f(\mathbb{I} - \mathbb{P}^{p} : \mathbb{C}^{s})^{-1}\right]^{-1}$$

$$\boldsymbol{\Sigma} = \mathbb{C}^{hom} : \boldsymbol{E}^{e} \quad , \quad \mathbb{C}^{hom} = \mathbb{C}^{pm} + \rho(\mathbb{C}^{i} - \mathbb{C}^{pm}) : \mathbb{A}^{i}$$

$$\mathbb{A}^{i} = \left(\mathbb{I} + \mathbb{P}^{i} : (\mathbb{C}^{i} - \mathbb{C}^{pm})\right)^{-1} : \left[(1-\rho)\mathbb{I} + \rho\left(\mathbb{I} + \mathbb{P}^{i} : (\mathbb{C}^{i} - \mathbb{C}^{pm})\right)^{-1}\right]^{-1}$$

$$P_{ijkl} = \frac{\partial}{\partial x_k x_l}\left(\int_D G_{ij}(\boldsymbol{x} - \boldsymbol{y})d\boldsymbol{y}\right), \forall \boldsymbol{x} \in D$$

Homogenized macroscopic yield criterion for COx claystone

Solid phase obeying Drucker-Prager plastic criterion:

$$\phi^m(\tilde{\boldsymbol{\sigma}}) = \tilde{\sigma}_d + T(\tilde{\sigma}_m - h) \leq 0$$

After making two steps of nonlinear homogenization procedure (Shen et al. 2020; Zhao et al. 2022; Chen et al. 2023):

$$\Phi_p = \Theta_p \frac{\Sigma_{eq}^2}{h^2} + 2f\left(1 - \frac{\Sigma_m}{h}\right)\cosh\left(\sqrt{\frac{3}{2T^2}}\ln(1 - \frac{\Sigma_m}{h})\right) - \left(1 - \frac{\Sigma_m}{h}\right)^2 - \Theta_0 = 0$$

$$\Theta_p = \frac{\frac{1+2f/3}{T^2}\frac{2}{3} + \frac{4}{9}\rho(\frac{3f}{2T^2} - 1)}{\frac{4T^2-12f-9}{6T^2-13f-6}\rho + 1}$$

$$\Theta_0 = f^2 - (1-f)^2\frac{f\rho}{1 + \frac{2}{3}f}$$

Explicitly taking into account influences of porosity f and mineral inclusions fraction ρ on macroscopic plastic yielding and failure

Non-associated plastic flow rule

Plastic hardening due to plastic deformation of solid phase $\tilde{\epsilon}^p$:

$$T(\tilde{\epsilon}^p) = T_m - (T_m - T_0)e^{-b_p\tilde{\epsilon}^p}$$

Proper description of plastic volumetric deformation with a non-associated plastic flow rule:

$$\begin{aligned} G_p =& \Theta_g \frac{\Sigma_{eq}^2}{h^2} + 2f(1 - \frac{\Sigma_m}{h})\cosh(\sqrt{\frac{3}{2Tt}}\ln(1 - \frac{\Sigma_m}{h})) - (1 - \frac{\Sigma_m}{h})^2 \\ \Theta_g =& \frac{\frac{1+2f/3}{Tt}\frac{2}{3} + \frac{4}{9}\rho(\frac{3f}{2Tt} - 1)}{\frac{4Tt-12f-9}{6Tt-13f-6}\rho + 1}. \end{aligned}$$

with evolution of plastic dilation coefficient t:

$$t(\tilde{\epsilon}^p) = t_m - (t_m - t_0)e^{-b_t\tilde{\epsilon}^p}$$

The plastic flow rule:

$$\dot{\boldsymbol{E}}^p = \dot{\lambda}_p \frac{\partial G_p}{\partial \boldsymbol{\Sigma}}$$

Viscoplastic deformation - unified approach

Viscoplastic deformation seen as delayed plastic flow due to viscosity of clay matrix (Zhou et al. 2008; Zhao et al. 2022; Chen et al. 2023):

$$\Phi_{vp} = \Theta_{vp}\frac{\Sigma_{eq}^2}{h^2} + 2f\left(1-\frac{\Sigma_m}{h}\right)\cosh\left[\sqrt{\frac{3}{2T_{vp}^2}}\ln\left(1-\frac{\Sigma_m}{h}\right)\right] - \left(1-\frac{\Sigma_m}{h}\right)^2 - \Theta_0 \geq 0$$

$$\Theta_{vp} = \frac{\frac{1+2f/3}{T_{vp}^2}\frac{2}{3} + \frac{4}{9}\rho\left(\frac{3f}{2T_{vp}^2}-1\right)}{\frac{4T_{vp}^2-12f-9}{6T_{vp}^2-13f-6}\rho + 1}$$

Time-dependent viscoplastic hardening:

$$T_{vp}(\bar{\varepsilon}^p) = T_m - (T_m - T_0)e^{-b_{vp}\bar{\varepsilon}^p} \leq T_p(\bar{\varepsilon}^p)$$

Non-associated viscoplastic flow:

$$\dot{\boldsymbol{E}}^{vp} = \dot{\lambda}_{vp}\frac{\partial G_{vp}}{\partial \boldsymbol{\Sigma}} \quad , \quad \dot{\lambda}_{vp} = \frac{1}{\eta_{vp}}\left(\frac{\Phi_{vp}}{h^2}\right)^m$$

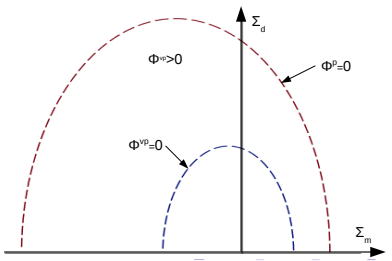

Anisotropy - waster sensitivity - thermal effects

Anisotropic effect on plasticity

- Material fabric tensor (Pietruszczak et al. 2000, 2001): A_{ij}
- Generalized loading orientation vector with respect to A_{ij}: $\boldsymbol{l} = (L_k/\sqrt{tr\boldsymbol{\sigma}^2})\boldsymbol{V}^k$
- Frictional coefficient of clay matrix depending on loading orientation defined by $\eta = a_{ij}l_il_j$:

$$T_m(\eta) = \hat{T}_m\left[1 + \hat{a}_{ij}l_il_j + c_1(\hat{a}_{ij}l_il_j)^2 + c_2(\hat{a}_{ij}l_il_j)^3 + ...\right]$$

Influences of waster saturation

$$E^s_{\perp}(p_{cp}) = E^s_{\perp 0}\left(1 + \beta_1\frac{p_{cp}}{h}\right)$$

$$\hat{T}_m(p_{cp}) = \hat{T}_{m0}\left(1 + \beta_2\frac{p_{cp}}{h}\right)$$

Thermal effect

$$\alpha = \alpha_{20-average}\left(1 + B\frac{\langle T - 20\rangle}{20}\right)$$

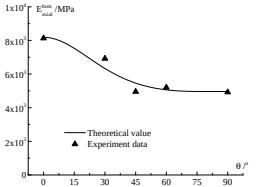

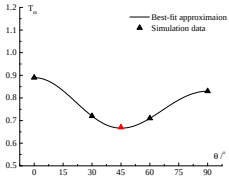

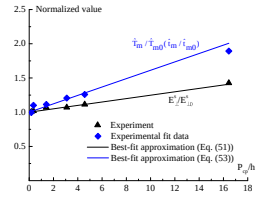

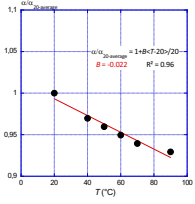

Stress-based hybrid formulation for saturated porous media

Elastic strain energy of cracked materials:

$$w_e(\boldsymbol{\varepsilon}, m, d) = g(d)\left\{\frac{1}{2}\boldsymbol{\varepsilon} : \mathbb{C}^0 : \boldsymbol{\varepsilon} - \left(\frac{m}{\rho_0^f}\right) M_0 \boldsymbol{B} : \boldsymbol{\epsilon} + \frac{1}{2} M_0 \left(\frac{m}{\rho_0^f}\right)^2\right\} + g_m^0 m$$

Driving energy for tensile crack:

$$\tilde{w}_e^0(\boldsymbol{\varepsilon}, p) = \frac{1}{2}\tilde{\boldsymbol{\sigma}}^b : \boldsymbol{\varepsilon} + \frac{1}{2}\frac{(p - p_0)^2}{M_0} \;\rightarrow\; \tilde{w}_{et}(\boldsymbol{\varepsilon}, p) = \frac{1}{2}\tilde{\boldsymbol{\sigma}}^{b+} : \boldsymbol{\varepsilon} + \alpha_d \frac{1}{2}\frac{(p - p_0)^2}{M_0}$$

An equivalent shear stress energy for shear cracks:

$$\bar{\tau} = \langle \frac{\langle \sigma_1^t \rangle_- - \langle \sigma_3^t \rangle_-}{2cos\varphi} + \frac{\langle \sigma_1^t \rangle_- + \langle \sigma_3^t \rangle_-}{2} tan\varphi - c \rangle_+$$

$$w_s = \frac{1}{2}\bar{\tau}\bar{\gamma} \;\;,\;\; \bar{\gamma} = \epsilon_1 - \epsilon_3$$

The plastic strain energy is decomposed into:

$$w_p = h_t(d^t) w_{pt}^0 + w_{ps}^0 \;\;,\;\; w_{pt}^0 = \int \boldsymbol{\sigma}^{pl+} : d\boldsymbol{\epsilon}^p \;\;,\;\; w_{ps}^0 = \int \boldsymbol{\sigma}^{pl-} : d\boldsymbol{\epsilon}^p$$

Analysis of laboratory heating tests-c

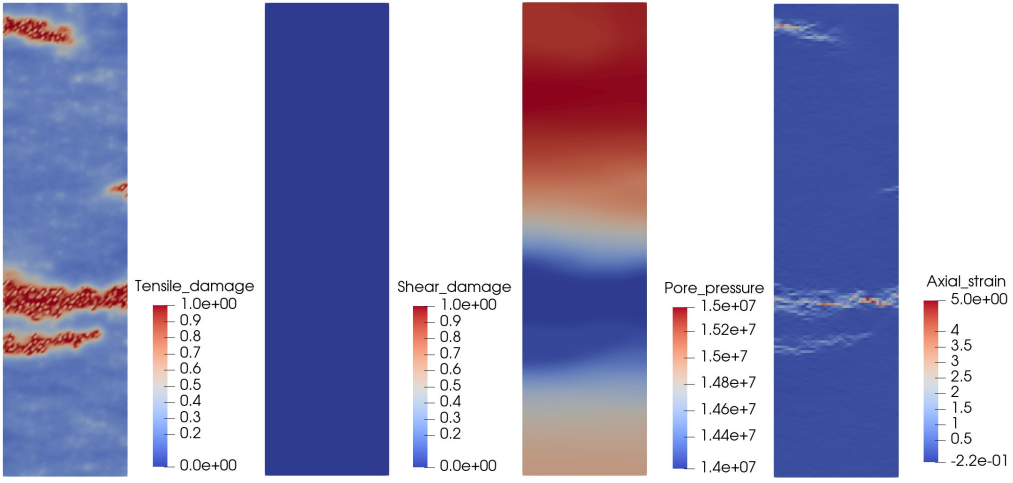

Distributions of tensile damage, shear damage, pore pressure and axial strain (in %) at the temperature value of $T_0 = 60°\mathrm{C}$

Swelling and self-sealing - example of experimental results

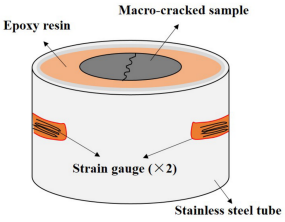

Experimental sample:
Steel-epoxy composite tube and a fractured COx sample
[C.WANG 2022]

Experimental procedure:

- Confining pressure: The sample was embedded in epoxy within a tube and subjected to 4 MPa confining pressure to replicate in-situ stress.
- Saturation and swelling: Synthetic water was injected 0.5 MPa from the bottom to saturate the sample, and swelling stress was recorded.

Experimental date: swelling pressure and permeability recovery

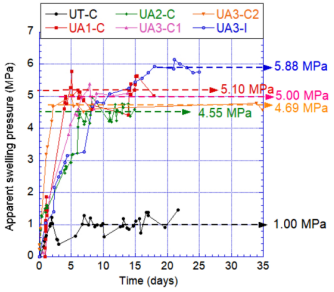

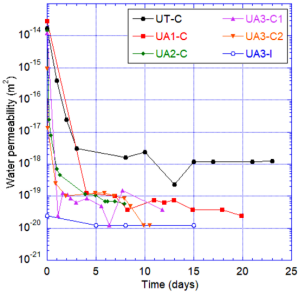

Swelling and self-sealing - numerical modeling

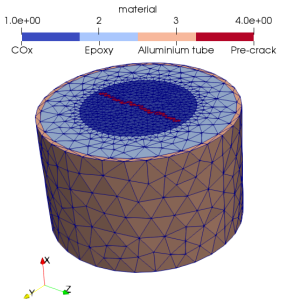

- **Material 1**: COx claystone
- **Material 2**: Epoxy resin (purely elastic)
- **Material 3**: Aluminum tube (purely elastic)
- **Material 4**: COx claystone with a pre-existing macrocrack

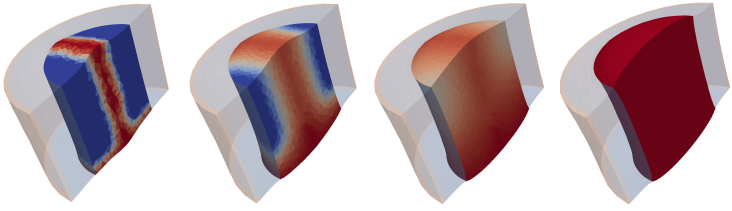

(j) 0 h (k) 20 h (l) 60 h (m) 100 h

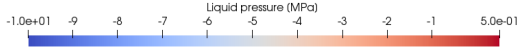

Evolution of liquid pressure in deformed COx sample after saturation; deformation magnified ×100

Swelling and self-sealing - comparison with experimental results

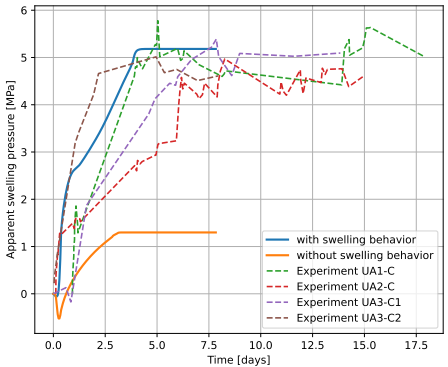

Comparison of apparent swelling pressure between experimental and the simulation results

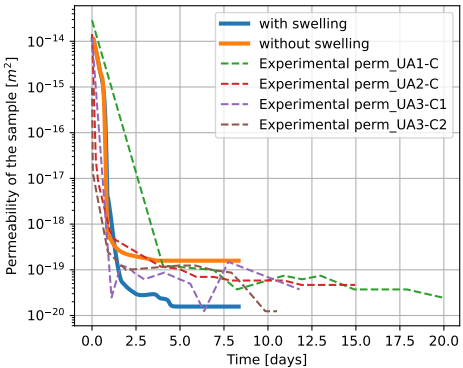

Comparison of permeability evolution with and without the swelling deformation

Concluding remarks

- Main results
  - Micro-structure based elastic-plastic modeling of heterogeneous clayey rocks;
  - Structural anisotropy, water sensitivity, thermal effect;
  - Damage and cracking
  - Efficient numerical solutions for both saturated and unsaturated porous media
  - Self-sealing of cracks;
  - Three-dimensional analysis of in-situ experiments
  - Application to design and optimization of sealing systems

- Open issues
  - A better description of permeability evolution with induced cracking;
  - Stronger coupling between thermal, hydraulic, deformation and cracking;
  - Very long term responses - PINNs based modeling
  - Modeling of the whole sealing systems - various materials and interfaces

Thank you for your attention !